Ecotoxicology and Environmental Safety 208 (2021) 111488

Contents lists available at ScienceDirect

Ecotoxicology and Environmental Safety

journal homepage: www.elsevier.com/locate/ecoenv

Research paper

# Evaluation of chemical stabilisation methods of coal-petcoke fly ash to reduce the mobility of Mo and Ni against environmental concerns

Patricia Córdoba *, Carlos Ayora, Xavier Querol

*Institute of Environmental Assessment and Water Research (IDÆA-CSIC), Spanish National Research Council, C/Jordi Girona 18-26, 08034 Barcelona, Spain*

ARTICLE INFO

Edited by Dr. R Pereira

*Keywords:*
Potential leaching
Fly ash
Adsorption capacity
Boiler slag
Aggregate product
Pollutants

ABSTRACT

Reducing the potential leaching of Mo and Ni from the fly ash (FA) of petroleum coke is an increasingly important issue as Asia and Europe's demand is expected to drastically intensify as continuing urbanisation and technological innovation demands ever more electricity. In the present study, we investigated coal combustion products (CCP) from a large coal-fired power station fed with a 56:44 coal/petroleum coke blend. Results revealed that leachable concentrations of Mo and Ni from FA were in the upper non-hazardous limit and in the inert limit, respectively (2003/33/EC). Whilst common prevention measures for Mo and Ni based on the adsorption capacity of boiler slag (BS), a mixture of BS: goethite, and jarosite, were considered insufficient to reduce the potential leaching of Mo into FA leachates, a novel chemical stabilisation method based on an aggregate product of portlandite and FA immobilised both Mo and Ni such that the resulting concentrations were below the limits established in the abovementioned 2003 EC Decision. Precipitation may be responsible for the fixation of Mo and Ni in the FA: portlandite aggregates as $Ca(MoO_4)$ and $NiMoO_4$, respectively. The findings of this novel study support the use of this aggregate to reduce FA pollutants, which will be of particular interest to nations that remain largely coal/petroleum coke-dependant.

## 1. Introduction

Currently, power generation is the second largest application of petroleum coke and this is likely to grow, particularly over the 2018–2025 period, as developing countries increasingly demand stable and reliable power generation infrastructure (Market Research Future, 2018). The cost-effectiveness of petroleum coke, along with its high carbon content, generates higher calorific values than coal. This has made it a prime candidate for firing power generation plants, leading to growing market demand from the power generation sector (Market Research Future, 2018).

Much of the petroleum coke used by emerging economies in Asia, such as in China and India, powers cement kilns or is used to generate electricity in power plants. Europe remains the second-highest importer of petroleum coke (Market Research Future, 2019), and despite the fact the European Union (EU) Member States have recently moved towards renewable-based energy systems, 21 EU Member States continue to use coal for power generation (Flisowska and Moore, 2019). As was observed in European power stations in the early 2000's, where up to 40% petroleum coke was added to the feed fuel (Izquierdo et al., 2007), a switch from coal to petroleum coke is not expected in countries that remain coal-dependant; rather a gradual increase of petroleum coke added to the fuel feed is predicted. This is a cause for concern as high petroleum coke combustion may increase sulphur dioxide ($SO_2$) emissions (Córdoba et al., 2012b; Wang et al., 2019). Owing to its high sulphur (S) content (3–8%), flue gas desulphurisation (FGD) must be available.

Co-firing petroleum coke may also modify the chemical environment of chlorine (Cl) because of the resultant high concentrations of hydrochloric (HCl) in the gaseous stream (Spears and Martínez-Tarrazona, 2004; Cui et al., 2018). For a large number of elements, an increase in the HCl concentration favours the formation of gaseous species, whereas increasing concentration of $SO_2$ in gas composition enhances the formation of sulphate condensed species (Díaz-Somoano et al., 2006). The organic affinity of elements such as, molybdenum (Mo), vanadium (V) and nickel (Ni) in petroleum coke favours their volatility during pulverised coal combustion (PCC) and later condensation into the finest fly ash (FA) particles (Córdoba et al., 2012b; Rodak et al., 2018). Indeed, previous research (Font et al., 2007) showed that a fuel blend with 30% petroleum coke, in comparison to a fuel blend with 4% petroleum coke,

* Corresponding author.
*E-mail address:* patricia.cordoba@idaea.csic.es (P. Córdoba).

https://doi.org/10.1016/j.ecoenv.2020.111488
Received 30 June 2020; Received in revised form 16 September 2020; Accepted 11 October 2020
Available online 26 October 2020

increased the volatility of Cl, fluorine (F), selenium (Se), S, thallium (Tl), tin (Sn), boron (B), and mercury (Hg), and enrichment of V, Ni, and Mo in FA.

Fly ash is composed of spherical high silicon–aluminium–calcium–potassium–iron–titanium–magnesium (Si–Al–Ca–K–Fe–Ti–Mg) vitreous particles with Fe-oxides and Al-Si species, irregular unburned coal and ash particles (Rask, 1985). Coal aluminous-silicate impurities, largely clays, with a much lower proportion of feldspars, melt during combustion to rapidly shape themselves into spherical droplets (Nugteren, 2010); other particles such as, calcite ($CaCO_3$), lime (CaO), quartz ($SiO_2$, mostly relict from coal), and gypsum ($CaSO_42H_2O$) are also formed.

A high concentration of CaO in FA causes alkalinity in pH in their leachates, which favours the mobility of elements, such Mo in its oxy-anionic form, and therefore, it may lead to environmental leaching problems that ultimately may reduce the reuse options of this solid residue. The EU's cut-off criteria (2003/33/EC) for the leaching of a number of elements, including Mo, and the criteria and procedures established for waste admission and landfills, was developed out of these concerns. The risk of excessively contaminating FA with trace pollutants is thus critical to the operation of a co-combustion power station and will directly affect the future social and economic development of still coal/petroleum coke-dependant countries.

In this study, we investigated the physical-chemical characteristics, including the leachability patterns of trace pollutants, of three coal combustion products (CCP): FA, boiler slag (BS), and FGD-gypsum, taken from a large coal-fired power station that co-fired petroleum-coke at high proportions (> 40%). The results are compared against established criteria for the leaching of CCP according to the 2003/33/EC Decision. Prevention measures based on novel chemical stabilisation methods, to reduce the mobility of elements such as Mo and Ni are critically evaluated against environmental concerns.

## 2. Materials and methods

### 2.1. Sample collection

Samples were collected in February 2018 over two consecutive days from a large co-combustion power station (1200 MW) in Spain, fired with 56:44 (%w/w) coal/petroleum coke.

In addition to the FA, BS, and FGD-gypsum, we analysed the effect of limestone (an alkaline sorbent used in the FGD process). The samples of FA (10 kg), BS (10 kg), limestone (5 kg) and FGD-gypsum (10 kg) were homogenised, dried (60ºC) and split into portions for further analysis. A portion of each homogenised solid sample was then separated and air-dried (at lab temperature) for Hg analysis.

### 2.2. Physical-chemical analyses

A dried portion was acid-digested in duplicate with a special two-step digestion method devised by Querol et al. (1993) to retain volatile elements. This consisted of weighing a ca. 0.1 g powdered sample into a PFTE vial and adding Primar grade concentrated HNO3 to predigest the organic fraction. This was followed with the addition of a concentrated Primar grade HF: HNO3:HClO4 mixture and evaporation on a hot plate at 240ºC, the purpose being digestion of all mineral phases. A number of reagent blanks and the standard reference materials NIST SRM 1633b (FA) and SARM 19 (South African coal, Council for Mineral Technology) were also digested to determine the accuracy of the analytical and digestion methods. Analytical precision of 2 NIST SRM 1633b samples, expressed as a relative error percentage (ER), were estimated at 2–9% for the majority of elements, and at around 18% for Cd with respect to certified values. The analytical precision of 2 SARM 19 samples were estimated at 2–9% for the majority of elements, with the exception of B, zinc (Zn), Ti, rubidium (Rb), germanium (Ge), and strontium (Sr), (7%<ER<16%). Concentrations of major elements in the acid digests were determined using Inductively-Coupled Plasma Atomic-Emission Spectrometry (ICP-AES, Iris Advantage Radial ER/S device from Thermo Jarrell-Ash). Trace elements were analysed by Inductively-Coupled Plasma Mass Spectrometry (ICP-MS, X-SERIES II Thermo Fisher Scientific, Thermo Fisher Scientific, Waltham, Massachusetts, EEUU) equipped with a Helium gas reaction/collision cell (CRC) to remove spectral interferences and used 10 μg/L In as the internal standard (MilliporeSigma is a German chemical, before 2014 known as Sigma-Aldrich, owned by Merck KGaA, St.Louis, Missouri, EEUU) to monitor and correct fluctuations in the signal both in the short and long term and to correct the effects of unspecified matrices.

Additionally, mercury (Hg) analyses were directly carried out on solid samples using a LECO AMA 254 Gold Amalgam Atomic Absorption Spectrometer (GA-AAS).

Powder X-Ray Diffraction (XRD) data were collected using a Bruker D8 A25 Advance, θ-θ diffractometer, with CuKα1 radiation, Bragg-Brentano geometry, and a position sensitive LynxEyeXE detector. Diffractograms were obtained at 40 kV and 40 mA, scanning from 4° to 60° of 2θ with a step size of 0.019°, and a counting time of 0.1 s/step to keep the sample in rotation (15/min). Crystalline phase identification was carried out using EVA software package (Bruker).

The particle resolved composition and morphology of FA was explored using a field emission scanning electron microscope (FESEM) J7100 with an energy-dispersive X-ray analyser (SEM-EDX). The grain size distribution of FA was determined by means of a laser light-scattering-based particle size, MALVERN Hydro 2000MU, with a working range of 0.2–1000 μm.

Leaching tests evaluated leachability patterns of trace pollutants in view of their future disposal in landfills. Analyses referred to the EN12457- 4 (14) standard set out by the EU (2003/33/EC) were applied to the by-products: BS, FA and FGD-gypsums. This consisted of a single batch leaching test that used Milli-Q (MQ) water as the leaching agent at an L/S (liquid to solid) ratio of 10 L/kg and 24 h of agitation time in an orbital shaker. Duplicated samples and blanks were prepared in a similar manner. The leachates were filtered through 0.45 μm filters and divided into two aliquots in High Density Polyethylene (HDPE) bottles. One aliquot was used for determination of pH and major anions, while the other was acidified with 1% $HNO_3$ for further analysis of major and trace metals using ICP-MS.

### 2.3. Estimation of the adsorption capacity of goethite and boiler slag for Mo and Ni

Evaluation of goethite (α-FeO(OH)) adsorption capacity for Mo and Ni relies on the fact that the chemical nature and high specific surface area of Fe oxides, including goethite and hematite ($Fe_2O_3$), make these oxides efficient sinks for many contaminants, including both cations and anions (Jeong et al., 2007).

Similarly, the estimation of BS adsorption capacity for Mo and Ni was proposed as a valorisation measure for BS due to its relatively high Fe content (6.3% as $Fe_2O_3$); this is for the reason that Fe species such as hematite are efficient sinks for metals. Certainly, enrichments of Mo in sediments are often attributed to adsorption into Fe and Mn oxides (Kaback and Runnels, 1980; Barling and Anbar, 2004; Chappaz et al., 2008; Goldberg et al., 2009) in which sorption of molybdate ($MoO_4^{2-}$) to Fe oxides usually increases with decreasing pH, however exhibit a weak maximum at around pH 4–5 (Goldberg et al., 1996; Gustafsson, 2003).

The selection of both goethite and BS to estimate their potential adsorption capacity for Mo and Ni, also relies on the fact that such a measure would not entail extensive investment for the power station and/or, globally, for the industrial sector as goethite is commonly formed by the weathering of the pyrite in acid drainage of coal piles and BS is a solid by-product generated during coal combustion. Analytical grade goethite (> 95%), supplied by Sigma Aldrich, and the BS collected from the power station were used in these experiments.

Two batch adsorption experiments of nine aliquots each were used to

estimate the BS and BS: goethite mixture adsorption capacity, respectively, for Mo and Ni. The aliquots contained a Ni and Mo dissolution/BS and a Ni and Mo dissolution/BS: goethite, respectively, both with a liquid-to-solid (L/S) ratio of 1. The Ni and Mo dissolution was prepared from $NiCl_26H_2O$ and $(NH_4)_4MoO_44H_2O$, respectively, to obtain a final concentration of 2 mg/L of Ni and 4.2 mg/L of Mo (6.0 ± 0.2 pH), while a BS sample (<1 mm particle size) and a mixture of BS and goethite (additional 20% of goethite in relation to BS), were used. Following preparation of the two series of aliquots, they were first acidified using 1% $HNO_3$ y $NH_4NO_3$ 0.05 M until reaching pH values between 4.0 and 8.0, agitated for 24 h, and then further centrifuged at 4000 rpm for 15 min. After centrifugation, the supernatants were filtered through 0.45 μm filters and divided into two aliquots in HDPE bottles. ICP-AES was then used to determine the concentration of Mo and Ni.

In these experiments we studied the adsorption capacity of BS and the mixture of BS: goethite for Ni and Mo, with the aim of determining both the minimum residence time for adsorption to occur, and the adsorption isotherm. The latter explores the distribution coefficient of Ni and Mo between the solution and the BS ( ± $Fe_2O_3$), thus determining the maximum capacity of adsorption.

Adsorption of Ni and Mo (% adsorption) by BS and by the mixture of BS and goethite was evaluated as per Eq. (1):

$$A = \frac{C_0 - C_f}{c_0} \cdot *100 \quad (1)$$

in which $C_0$ is the initial concentration of Ni and Mo, respectively, Cf is the concentration in the equilibrium solution or final solution.

### 2.4. Estimation of the adsorption capacity of jarosite for Mo in a batch reactor with $CO_2$ injection

As a goethite, jarosite ($KFe_3^{3+}(SO_4)_2(OH)_6$) is commonly formed by

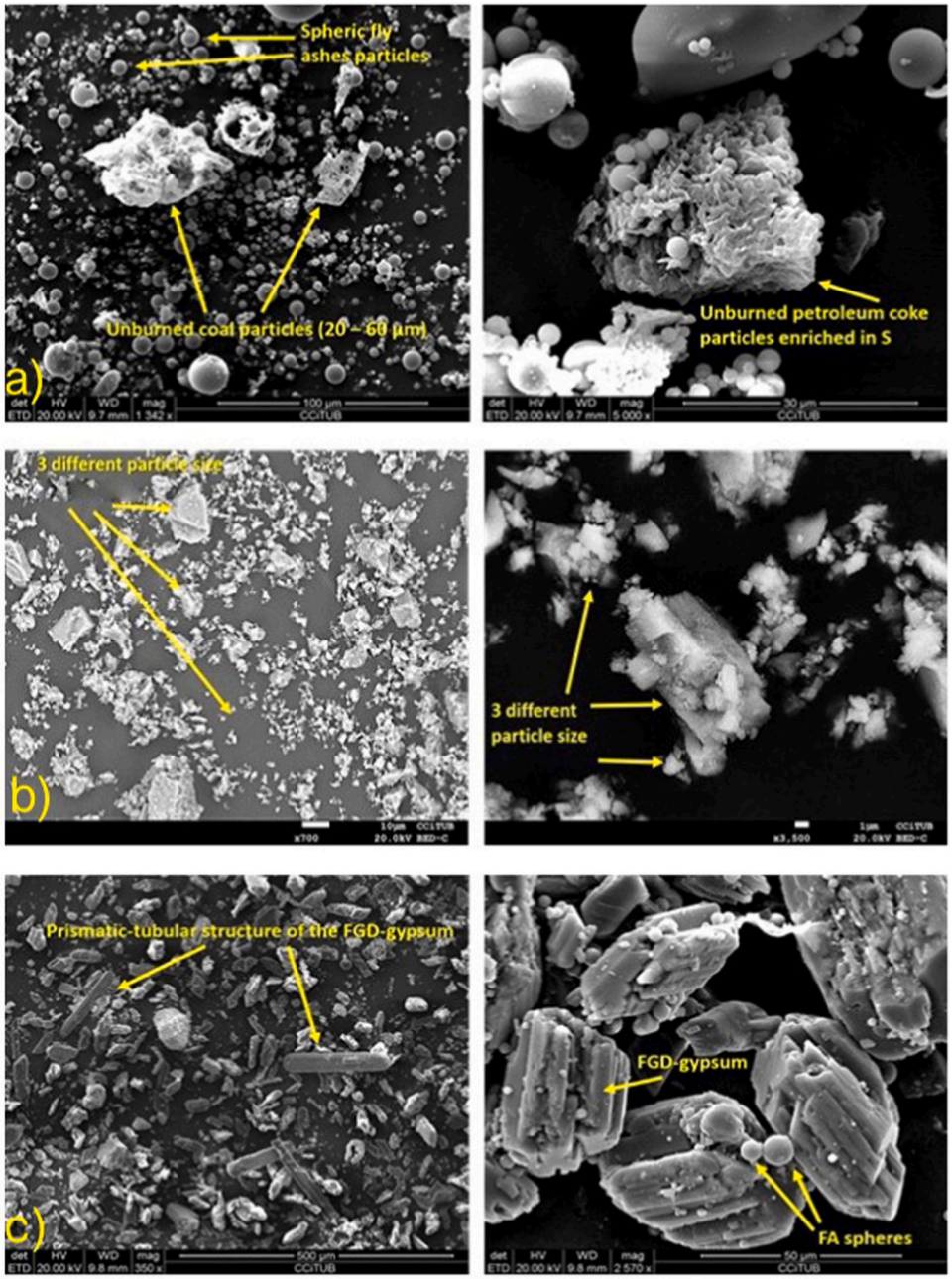


**Fig. 1.** Scanning electron microscope (SEM) photomicrographs of fly ash (a), limestone (b), and FGD-gypsum prismatic-tubular structure (c).

the weathering of pyrite formed in acid drainage of coal piles and its chemical nature and high specific surface area make this mineral an efficient sink for many contaminants.

Utilising the adsorption preliminary results, adsorption capacity of jarosite for Mo in a batch reactor with $CO_2$ injection was also estimated. The premise of this experimental work relies on the fact that an alkaline pH of the FA leachates would favour the mobility and leaching of Mo oxyanionic species, while adsorption of Mo by a sorbent would only obtain significance at pH< 4.5. Therefore, our experimental purpose is to evaluate the influence of $CO_2$ bubbling along with the concomitant pH drop on Mo removal from FA leachate via sorption processes where Mo could likely be removed in non-jarosite forms. This estimate method for the potential adsorption capacity of Mo and Ni, also relies on the fact that $CO_2$ is also an excess gas (released during coal combustion) in coal-fired power stations, therefore, such a measure would not entail high investment for the power station, or globally, for the industrial sector.

To this end, to boost the gas mass transfer, FA leachates were transferred into a glass vessel (Fig. S1) that was then placed over a magnetic stirrer. pH was continuously measured with the insertion of a pH probe into the vessel. The $CO_2$ gas flow (gas cylinder) bubbled through a porous, sintered glass bubbler, using inlet ports, into the closed, stirred vessel, which provided the unit for the $CO_2$ mass transfer from the gas to the aqueous phase of the leachates. The vessel was charged initially with a scaled volume of leachates (~250 mL), and an incremental dosage of the jarosite was added into the vessel while bubbling the $CO_2$ (Fig. 1). Once the target pH was achieved, while maintaining the injection of $CO_2$ (to avoid the restoration of the pH), incremental dosages of jarosite were added to promote Mo adsorption. A proportion of $CO_2$ was vented to avoid pressurising the vessel.

A total of three experiments were carried to evaluate the adsorption capacity of jarosite for Mo in a batch reactor. First, we assessed the variation rate of pH as a function of $PCO_2$ in the reactor, and reaction time. Second, we analysed $PCO_2$ and the reaction time needed to achieve the target pH. Third, we assessed the adsorption capacity of jarosite for Mo and the jarosite/FA dose in the batch reactor.

The jarosite used in these experiments was collected from mine waste deposits in Rio Tinto, Huelva, Spain. Río Tinto has the essential geochemical conditions for the precipitation not only of jarosite, but also of other ferric sulphate minerals such as copiapite, schwertmannite, etc.

### 2.5. Reduction of the Mo and Ni potential leaching by aggregate mixtures

Aggregate mixtures were also tested for their potential to reduce Mo and Ni leaching in FA leachates. Our objective was to determine whether an aggregate product consisting of FA and another material (Lieberman et al., 2018) could lead to the fixation/immobilisation of Mo and Ni, respectively, thus reducing the potential leaching of both elements into the FA leachates.

In addition to the limestone ($CaCO_3$) and FGD-gypsum ($CaSO_4 2H_2O$) from the coal-fired power station, portlandite ($Ca(OH)_2$) powder was also used as material for the aggregate mixtures. Portlandite of analytical grade (> 95%), supplied by Sigma Aldrich, was used in aggregate product mixes. Aggregates each contained one of the three materials mixed with FA in varying ratios; this was achieved using a temperature-controlled batch reactor with a mechanical stirrer. The aggregates with their respective replicates were prepared according to the ratios presented as supporting information (Table S1).

Prior to fixation, FA was homogenised for uniformity by mixing the aggregates for 25 min at 250 rpm while adding 25–40% Milli-Q water. The slurry aggregate mixture was transferred into the batch reactor where it was stirred for four hours. Following agitation, 50 mL of the aggregate mixture was filtered and divided into two aliquots. One aliquot was acidified to 1% $HNO_3$ and stored for the Mo and Ni quantification analyses conducted using ICP-MS; another was stored for pH and conductivity readings; the remaining aggregate was left to dry in an oven for 10 h at 50 °C. A portion of the resulting solid product, hereinafter referred to as 'aggregate', was analysed with SEM-EDX to identify a possible formations of Ni and Mo-solid phases, while the remainder was used for leaching tests. Leaching tests were conducted at an L/S ratio of 10 L/kg and received 24 h of agitation time in an orbital shaker, the purpose of which was to evaluate FA against the cut-off points stipulated in the EN12457- 4 standard that resulted from the EU's decision (2003/33/EC).

## 3. Results and discussion

### 3.1. Physic-chemical characterisation

#### 3.1.1. Characterisation of fly ash and boiler slag

FA principally consisted of an amorphous aluminium-silicate glass matrix with mullite ($Al_6Si_2O_{13}$) and quartz ($SiO_2$) (Fig. S2a).

FA was characterised by a lognormal and tri-modal distribution with two partially overlapping coarse modes around 12 and 60 μm, and a fine mode around 1 μm (Fig. S3a). SEM results indicate that the coarse mode may reflect the presence of unburned C particles (Fig. 1a). Due to a reduced concentration of ash and to its lower char reactivity, the concentration of unburned carbon particles in FA from petroleum-coke-fired combustors is generally higher than in FA from straight coal firing (Bryers, 1995).

FA composition is largely a result of the feed fuel and the relative contribution of each component in the blend. Petroleum coke, which generally has low quantities of trace elements, exerted a dilution effect in the concentration of coal-derived elements in the FA (Table 1), with the exception of those distinctively enriched by petroleum coke. Thus, FA was enriched by S (by a factor of 1.3), in V (13), Ni (7.6) and Mo (1 4 0), with respect to the average values for 25 EU coal FA (Moreno et al., 2005). A 2- to 10-fold increase between FA sampled in 2005 to samples taken between 2007 and 2008 (Córdoba et al., 2012) was also noted, which may reflect shifting coal/petroleum coke ratios over time to reduce cost.

Similar to FA, BS was characterised by the predominance of an aluminosilicate glass matrix that contains relatively low concentrations of mullite and quartz (Fig. S2b); BS also demonstrated high concentrations of V and Ni (Table 1). Previous studies on the partitioning and speciation of trace elements at this co-combustion station found no evidence of enrichment of trace elements in BS (Córdoba et al., 2012). This difference is likely due to the substantially greater petroleum coke proportions being currently fired.

#### 3.1.2. Characterisation of limestone and FGD-gypsum

The limestone used at the power station was principally calcite (Fig. S2d); it was characterised by a lognormal and bi-modal distribution with a predominant fine (max 3 μm) and coarse (max 30–40 μm) mode that resulted in fine particle sizes (Fig. S3b). SEM-EDX analysis of limestone (Fig. 1b) provided evidence for three particle sizes of limestone and limestone particles < 10 μm. Notable concentrations of Sr (898 mg/kg), Mn (59 mg/kg) and U (1.8 mg/kg), were also observed (Table 1).

Gypsum with minor concentrations of calcite was the main crystalline phase detected in FGD-gypsum (Fig. S2c). The FGD-gypsum presents a lognormal particle size distribution with a predominant mode ranging from 40 to 50 μm and two fine modes of around 1 μm and 10 μm (Fig. S3c). SEM-EDX analyses (Fig. 1c) show the characteristic prismatic-tubular structure of FGD-gypsum with a substantial quantity of FA spheres and FA-associated Mg, Al, and Si particles (<5 μm) evident on the surface.

FGD-gypsum demonstrated substantial concentrations of Mn (201 mg/kg), Sr (627 mg/kg), Ti (42 mg/kg), and V (25 mg/kg) (Table 1). The alkaline pH of both FA and the limestone slurry may have promoted the dissolution of these and other elements (i.e. Se, As, Sb and V) in both the limestone and gypsum slurry when flue gas passes through the sprayers. These elements tend to precipitate or co-precipitate in the

**Table 1**
Concentration of major, minor and trace elements in the fly ash, boiler slag, limestone, and FGD-gypsum.

| % | Fly ash | Boiler Slag | Limestone | FGD-gypsum |
|---|---|---|---|---|
| $Al_2O_3$ | 27 | 25 | 0.04 | 0.1 |
| CaO | 1.9 | 1.8 | 51 | 31 |
| $Fe_2O_3$ | 7.0 | 6.3 | 0.03 | 0.1 |
| $K_2O$ | 4.2 | 3.8 | < 0.01 | < 0.01 |
| MgO | 1.7 | 1.6 | 0.3 | 0.9 |
| $Na_2O$ | 0.7 | 0.7 | 0.001 | 0.03 |
| $SO_3$ | 1.1 | 0.2 | 0.04 | 42 |
| mg/kg | | | | |
| Hg | 0.1 | 0.001 | 0.004 | 1.0 |
| Li | 172 | 152 | < 0.01 | 2.2 |
| Be | 4.8 | 4.6 | < 0.01 | < 0.01 |
| B | 276 | 860 | 120 | 155 |
| Sc | 29 | 29 | < 0.01 | < 0.01 |
| Ti | 6109 | 5534 | 18 | 42 |
| V | 3173 | 3035 | 2.8 | 25 |
| Cr | 266 | 212 | < 0.01 | 1.6 |
| Mn | 471 | 410 | 59 | 201 |
| Co | 32 | 24 | < 0.01 | 0.4 |
| Ni | 883 | 686 | 4.5 | 9.1 |
| Cu | 99 | 48 | 1.2 | 2.2 |
| Zn | 232 | 47 | 5.4 | 12 |
| Ga | 42 | 10 | < 0.01 | < 0.01 |
| Ge | 3.4 | 0.4 | < 0.01 | < 0.01 |
| As | 100 | 3.8 | 1.0 | 1.6 |
| Se | 3.0 | 1.5 | < 0.01 | 1.1 |
| Rb | 179 | 164 | < 0.01 | 1.3 |
| Sr | 348 | 323 | 898 | 627 |
| Y | 44 | 40 | 3.0 | 2.1 |
| Zr | 188 | 196 | < 0.01 | 0.2 |
| Nb | 20 | 18 | < 0.01 | < 0.01 |
| Mo | 63 | 15 | < 0.01 | 0.9 |
| Cd | 1.0 | < 0.01 | < 0.01 | < 0.01 |
| Sn | 7.6 | 6.7 | < 0.01 | 2.0 |
| Sb | 25 | 3.5 | < 0.01 | < 0.01 |
| Cs | 26 | 23 | < 0.01 | < 0.01 |
| Ba | 1688 | 1483 | 2.9 | 11 |
| La | 72 | 68 | 0.9 | 0.9 |
| Ce | 129 | 124 | 0.9 | 1.2 |
| Pr | 16 | 14 | < 0.01 | < 0.01 |
| Nd | 61 | 56 | < 0.01 | < 0.01 |
| Sm | 12 | 11 | < 0.01 | < 0.01 |
| Eu | 2.7 | 2.5 | < 0.01 | < 0.01 |
| Dy | 9.7 | 8.8 | < 0.01 | < 0.01 |
| Ho | 1.9 | 1.7 | < 0.01 | < 0.01 |
| Er | 5.3 | 4.7 | < 0.01 | < 0.01 |
| Ta | 1.8 | 1.8 | < 0.01 | < 0.01 |
| W | 5.6 | 2.1 | < 0.01 | < 0.01 |
| Tl | 2.4 | < 0.01 | < 0.01 | < 0.01 |
| Pb | 92 | 13 | 1.0 | 1.4 |
| Bi | 1.6 | < 0.01 | < 0.01 | < 0.01 |
| Th | 29 | 27 | < 0.01 | < 0.01 |
| U | 8.3 | 7.5 | 1.8 | 1.4 |

FGD-gypsum upon reaching saturation in the aqueous phase of the gypsum slurry.

### 3.1.3. Potential leaching of fly ash

Distinctions identified in the leaching results compared against the waste acceptance criteria for landfills, reveals that Mo (16 mg/kg) in FA leachates is higher than the non-hazardous limit (10 mg/kg) established by the European Council Decision (2003/33/EC). This supports the development of prevention measures to reduce the potential leaching of Mo (Table 2).

Levels of nickel (1.6 mg/kg) and Se (0.3 mg/kg) in FA leachates exceed the inert limit while As (3.8 mg/kg) exceeds the one of the non-hazardous limit (Table 2) established by the European Council Decision (2003/33/EC), which also recommends that As and Se leaching should be reduced in order to meet future new standards. Antimony (0.8 mg/kg) was also higher than that the non-hazardous limit (0.7 mg/kg) but far below the criteria for hazardous waste (Table 2). As for As and Se, recommendations from the European Council Decision (2003/33/EC) support the development of prevention measures to reduce the potential leaching of Sb in order to meet future new standards.

Levels of pollutants in both the BS and FGD-gypsum samples were within the limits to be accepted at non-hazardous waste landfills. However, it should be stressed that the leaching values of Mo and particularly of Se in the FGD-gypsum were close to and within the inert range, respectively. $SO_4^{2-}$ leach levels from the FGD-gypsums fell in the range of inert material, however with values close to that of non-hazardous waste. Given that the leaching behaviour of $SO_4^{2-}$ is related to the solubility of gypsum, developing prevention measures is not currently possible.

### 3.2. The adsorption capacity of boiler slag and goethite for Mo and Ni

Fig. 2 shows the behaviour of Mo and Ni after 24 h in contact with a BS and the BS: goethite mix, respectively.

Considering that the target concentrations of both Ni (2.1 mg/L) and Mo (4.8 mg/L) in the synthetic aliquots were set at a pH of 6.0 ± 0.2 (starting adsorption point), a slight increase of Ni concentration in the aliquots of the two batch adsorption experiments at pH< 6.0 was observed. This could be ascribed to the dissolution of BS components. In further detail, BS is characterised by a relatively high concentration of Ni (686 mg/kg), which highlights that, despite its relatively high content in Fe (6.3% as $Fe_2O_3$), its exposure to relatively acidic conditions could lead to an increase of Ni concentrations as a result of BS leaching. In fact, the slight increase in Ni concentration in the aliquots with 4.0–4.5 pH between, would have resulted in negative adsorption for both BS and the BS: goethite mix, indicating that Ni is not relevant to goethite adsorption.

The adsorption of Ni in the solid phase of BS and BS: goethite could

**Table 2**
Leachable concentrations of elements in fly ash and comparison against established criteria for the leaching of CCP according to the 2003/33/EC Decision (mg/kg).

| | | | | EC/33/2003 DECISION | | |
|---|---|---|---|---|---|---|
| | Fly ash | Boiler Slag | FGD-gypsum | Inert | Non-hazardous | Hazardous |
| pH | 8.2 | 7.7 | 8.6 | | < 6 | |
| K (mS) | 62 | 1294 | 4321 | | | |
| F | 13 | 4.0 | 164 | 10 | 150 | 500 |
| Cl | < 30 | < 30 | 1922 | 800 | 15,000 | 25,000 |
| $SO_4^{2-}$ | 6735 | 113 | 30,385 | 1000 | 20,000 | 50,000 |
| Cr | 0.03 | < 0.01 | < 0.01 | 0.5 | 10 | 70 |
| Ni | 1.6 | 0.2 | 0.1 | 0.4 | 10 | 40 |
| Cu | 0.01 | < 0.01 | 0.04 | 2 | 50 | 100 |
| Zn | < 0.01 | < 0.01 | < 0.01 | 4 | 50 | 200 |
| As | 3.8 | 0.03 | 0.01 | 0.5 | 2 | 25 |
| Se | 0.3 | 0.01 | 0.1 | 0.1 | 0.5 | 7 |
| Mo | 16 | 0.1 | 1.2 | 0.5 | 10 | 30 |
| Sb | 0.8 | < 0.01 | 0.01 | 0.06 | 0.7 | 5 |

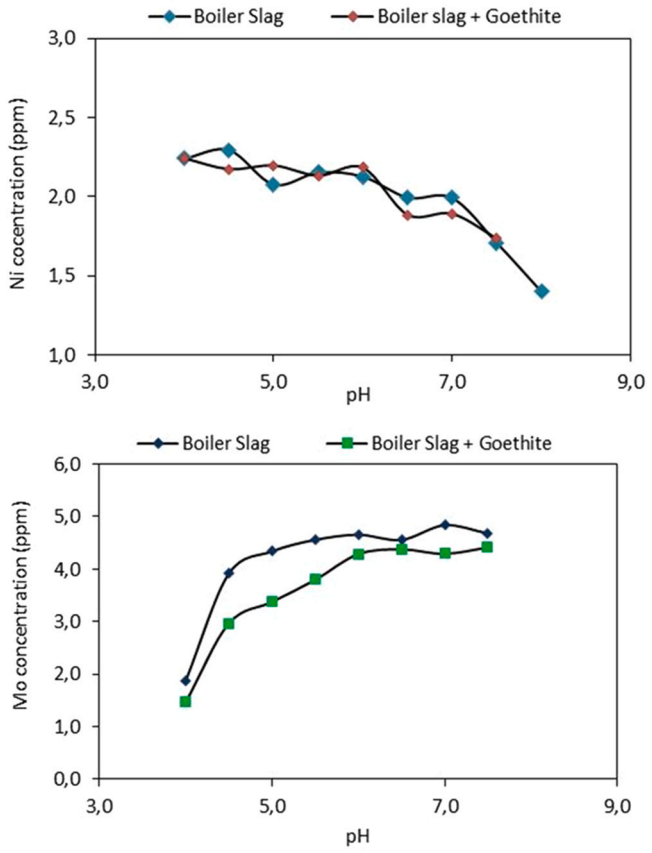


**Fig. 2.** Behaviour of Mo (top) and Ni (bottom) in contact with boiler slag and a boiler slag: goethite mixture as pH function.

be significant at a pH > 7.5, in which Ni would be expected to be largely dissolved as $Ni^{2+}$ and subsequently, could be adsorbed in protonated solutions.

Similarly, in the aliquots of the two batch adsorption experiments, Mo concentration increased at 7.0–7.5 pH, which could largely be ascribed to the dissolution of BS and/or Mo impurities in the samples. As opposed to Ni, no negative adsorption results for Mo would be expected to have been observed, rather the concentration of Mo would decrease sharply at pH< 5.0. This behaviour is aligned with the predominant specie of Mo in an aqueous solution, in which it is mostly dissolved as an oxyanion $MoO_4^{3-}$ and could then be adsorbed in protonated surfaces (positive charged). However, in these experiments, despite the preliminary positive adsorption results, we cannot confirm that Mo is adsorbed by BS or by the BS: goethite mix. Molybdenum could precipitate as an X-$MoO_4^{3-}$ solid phase per se, co-precipitate on the BS and/or goethite surface, and/or be absorbed by BS and/or the BS: goethite mix. However, the findings have contributed to our understanding of the behaviour of Ni and Mo in aqueous solutions.

### 3.3. The adsorption of jarosite for Mo in a batch reactor with $CO_2$ injection

#### 3.3.1. Rate of pH decrease in fly ash leachates

As expected, the pH of the FA leachates decreased with the injection of $CO_2$ (0.5 bar) (Table S2). The diffusion of $CO_2$ from gas to the aqueous phase provoked $CO_2$ hydrolysis, which decreased the pH of the FA leachate.

Fifteen minutes following the reaction, the gradual increase of the $CO_2$ partial pressure (0.5–1.2 bar) into the batch reactor did not cause a large drop of the leachate's pH, rather it remained stable at around 4.5. This was considered to be due to equilibrium conditions between the aqueous phase of FA leachate and atmospheric $CO_2$. These findings supported our conclusions that, i) the minimum pH value that can be reached in these experiments is ~ 4.5, therefore, reaching a pH below this value is a critical point, and ii) the pH of FA leachate followed a sharp decrease during the initial minutes (15 min) of $CO_2$ injection, and later stabilised at around 4.5 owing to equilibrium conditions (70–80 min).

#### 3.3.2. Adsorption capacity of Mo on jarosite in a batch reactor with $CO_2$ injection

Fig. 3 illustrates that the adsorption behaviour of Mo does not follow a regular pattern. Five minutes after the initial addition of jarosite (initiation at the target pH of 4.5), Mo concentration marginally increased in FA leachates; this could not be ascribed to jarosite, rather to a factor of the experimental analysis. From that point on, the progressive addition of jarosite provided a sufficient surface to induce the adsorption of Mo, reaching a maximum of 50% adsorption (Fig. 3). Subsequently, jarosite adsorption of Mo decreased. In this dynamic context in which $CO_2$ was continuing to be injected in order to avoid the restoration of FA pH, there could have been competition between $CO_2$ gas molecules and leachable Mo for the jarosite surface, which would explain the reduced Mo adsorption observed.

To our understanding, reduced Mo adsorption on the jarosite surface could be the result of an initial physical adsorption of Mo on the jarosite surface followed by a saturation of the available voids, either by $CO_2$ gas molecules and/or by Mo; this would explain increased Mo concentration in FA leachates (Mo desorption). Considering that jarosite, in these experiments, does not demonstrate a reliable adsorption capacity for Mo, we disregarded jarosite as an option to reduce the potential leaching of Mo in the FA leachates under study.

The adsorption capacity of Mo on jarosite in a batch reactor with $CO_2$ injection as function of time is provided as supplemental information (Fig. S4).

### 3.4. Fixation of Mo and Ni by aggregate mixes

#### 3.4.1. Fixation of Mo and Ni in the fly ash: limestone aggregate

Table 3 shows Mo and Ni concentrations in the leachates of the fly ash: limestone aggregate product.

Results demonstrate that the FA and limestone aggregates, regardless of the proportions of the mix, did not provide enough fixation or immobilisation of Mo to reduce its concentration in the leachate under the limits established by the European Council Decision (2003/33/EC). In the case of Ni, the fly ash: limestone aggregates reduced the concentration of Ni in FA leachates within the limit established (0.4 mg/kg) (2003/33/EC).

SEM-EDX analysis of the fly ash: limestone aggregate product

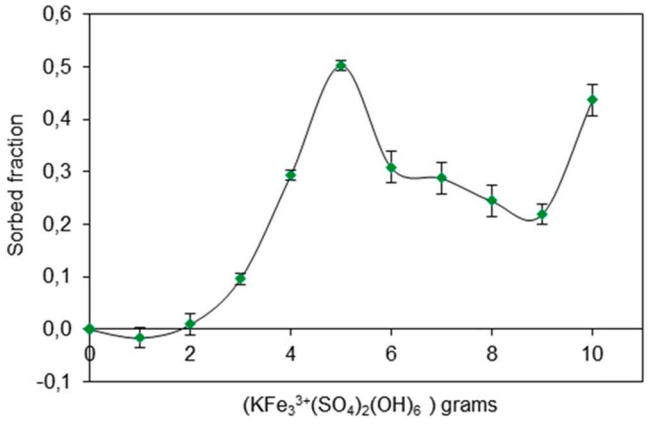


**Fig. 3.** Experimental adsorption of leachable Mo from fly ash on jarosite surface.

**Table 3**
Leachable concentrations of Ni and Mo (mg/kg) from the aggregate products following the standard EN12457- 4.

| Aggregate product mixture | leachate pH | Mo [mg/kg] | Ni [mg/kg] | As [mg/kg] | Se[mg/kg] |
|---|---|---|---|---|---|
| Fly ash | 7.34 | 16 | 1.6 | 3.8 | 0.3 |
| FA:$CaCO_3$ (1:0.25) | 9.19 | 12 | 0.4 | 2.2 | 0.07 |
| FA:$CaCO_3$ (1:0.5) | 8.06 | 10 | 0.3 | 2.4 | 0.09 |
| FA:$CaCO_3$ (1:1) | 8.16 | 14 | 0.4 | 2.0 | 0.08 |
| FA:FGD-gypsum (1:0.25) | 8.27 | 14 | 3.4 | 1.4 | 0.1 |
| FA:FGD-gypsum (1:0.5) | 8.13 | 12 | 2.0 | 1.8 | 0.1 |
| FA:FGD-gypsum (1:1) | 7.98 | 13 | 2.8 | 1.0 | 0.1 |
| FA:$Ca(OH)_2$ (1:0.25) | 12.45 | 10 | 0.2 | 0.8 | 0.07 |
| FA:$Ca(OH)_2$ (1:0.5) | 12.44 | 9.9 | 0.1 | 0.6 | 0.04 |
| FA:$Ca(OH)_2$ (1:1) | 12.50 | 4.5 | 0.01 | 0.3 | 0.01 |

(Fig. S5a) evidenced the occurrence of a substantial quantity of residual calcite and FA spheres. No Ni-solid phases were identified; this may have been owing to the already low concentration of Ni in the leachates compared to the principal FA components. According to solubility data in the Wateq4f database (Parkhurst and Appelo, 1999) the three leachates are subsaturated in Ni solid phases ($NiCO_3$ and $Ni(OH)_2$), therefore Ni retention could be owing to sorption on surface of the aggregate particles. Indeed, Ni sorption on clay particles increases dramatically at pH levels higher than neutral (Baeyens and Bradbury, 1998).

### 3.4.2. Fixation of Mo and Ni in the fly ash: FGD-gypsum aggregates

Table 3 shows Mo and Ni concentrations in the leachates of the fly ash: FGD-gypsum aggregates. Results demonstrate that the FA: FGD-gypsum aggregates, regardless of the mixture ratio, did not provide enough Mo fixation or immobilisation to reduce concentration below the limits established (2003/33/EC). Moreover, the addition of FGD-gypsum in FA leachates provoked an increase of Ni concentration, which could be owing to the dissolution of Ni impurities from the FGD-gypsum. At this power station under study, the FGD utilizes a recirculation system that promotes the saturation of metal aqueous complexes following a number of water cycles into the scrubber.

SEM-EDX photomicrographs of the solid phase of the fly ash: FGD-gypsum aggregates (Fig. S5b) show a significant amount of residual FGD-gypsum ($CaSO_42H_2O$) and FA spheres; however, no Mo and/or Ni solid phases were identified.

### 3.4.3. Fixation of Mo and Ni by the fly ash: portlandite aggregates

Table 3 shows Mo and Ni concentrations in the leachates of fly ash: portlandite aggregates.

Results show that portlandite addition caused the immobilisation/fixation of Mo and Ni enough to reduce their concentration in the leachates to below the established limits (2003/33/EC).

The SEM photomicrograph of the solid phase of the fly ash: portlandite aggregates (Fig. 4) evidenced the occurrence of a Ca-Mo phase, which confirms the fixation/immobilisation of Mo with a solid phase. Assuming equilibrium with $Ca(OH)_2$ at a pH of 12.45, the leachates were largely oversaturated with $CaMoO_4$ (Felmy et al., 1992). Therefore, precipitation may be responsible for the fixation of Mo in the FA: portlandite aggregates. Furthermore, a possible electrostatic interaction of fine $Ca(MoO_4)$ precipitates, that have a positive zeta potential, with the alumina-silicate groups of the FA (having a negative zeta potential at that pH) (Lieberman et al., 2015) could have also resulted in the co-fixation of $Ca(MoO_4)$ precipitates on the FA surface.

On the other hand, while no Ni-solid phases were detected in the solid aggregates, the leachate pH was 12.45, and the Ni concentration was between 5 and 10 mg/L. According to the solubility data described

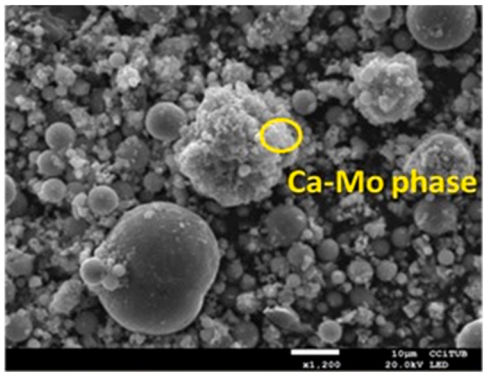


**Fig. 4.** SEM photomicrograph of the solid phase of the fly ash: portlandite aggregate product.

by Minteq4f (Parkhurst and Appelo, 1999), the leachates were largely oversaturated by $NiMoO_4$, favouring $NiMoO_4$ precipitation.

As for Mo and Ni, results demonstrate that the FA: portlandite aggregates provide enough As and Se fixation or immobilisation to reduce their concentrations below the limits established (2003/33/EC), which supports the use of this aggregate to reduce FA pollutants. The fixation/immobilisation of both As and Se could be attributed to the formation of low solubility of calcium arsenates ($Ca(AsO_4)_3$) and calcium selenates ($CaSeO_4$), respectively.

The immobilisation mechanisms of As and Se in this study are also in line with those exposed by Guo et al. (2019). In this work, authors investigated the influence of various Ca additives on the released of As and Se, among other pollutants, and indicated that the suppression of As and Se could be associated to the formation of low solubility of Ca $(AsO_4)_3$ and $CaSeO_4$ in association with the formation of ettringite ($Ca_6Al_2(SO_4)_3(OH)_{12}26H_2O$) and hydrocalumite ($3CaO{\cdot}Al_2O_3{\cdot}CaX_{2/m}$), which in turn, were the immobilisation mechanisms that prevent the release of other anionic pollutants (e.g. B, F, S, and Cr).

The formation of ettringite has also been associated to the suppression of As, B, and Se in FA leachates by Hartuti et al. (2017). In this study, authors examined the effects of the additives on suppressing As, B, and Se leaching from coal fly ash using $Ca(OH)_2$, paper sludge ashes, and filter cake and found that the leaching concentrations of As, B, and Se were greatly reduced in FA with the highest effect given by $Ca(OH)_2$, being the leached Ca and Na ions the key factors affecting the decrease of As, B, and Se leaching concentrations from FA.

In can, therefore, be conclude that Ca additions to As and Se-containing wastes and/or by-products have been proven to be beneficial in reducing the mobility of dissolved As and Se through the formation of calcium arsenates and selenates, respectively.

In this study, the resulting FA: portlandite aggregate product at this stage could be used as a substitute for concrete production, which would entail the end-step of the valorisation chain of this solid by-product. In our earlier works (Lieberman et al., 2018), we did evaluate the use an aggregate produced by mixing coal phosphate waste with FA and/or bivalve shells as a partial substitute for sand in concrete production. Results revealed an increase in the compressive strength of the concrete end-product by approximately 15% by partial replacement of sand with the aggregate product in comparison to the strength with no sand replacement. Reduced penetration of $Cl^-$ (tested by ASTM C1202) in the concrete end-product was also noticed by partial replacement of the sand by the aggregate product.

On the other hand, ashes from petroleum coke could also be used in the cement industry (Olmeda et al., 2013), or less often, in agriculture as soil acidity amendments (Anthony et al., 2003, 2006; Chen et al., 2010). The relatively high enrichment of FA in S, V, Ni, Mo, among others, may not be a restriction to their use in agriculture as demonstrated in a study performed by Chen et al. (2006) where petroleum coke ashes application

in some soils did not reach levels of these elements that might cause environmental problems.

## 4. Conclusions

Comparing the leaching results against the waste acceptance criteria at landfills revealed that the leachable concentrations of Mo and Ni in the fly ash were in the upper non-hazardous limit and in the inert limit, respectively established by the European Council Decision (2003/33/EC).

Experiments based on the adsorption capacity of a mixture of boiler slag: goethite showed that Ni adsorption is significant at a pH > 7.5, and Mo at a pH< 4.5, therefore findings indicate that the role of goethite in the adsorption of Mo and Ni is not relevant. The results of this study also failed to support jarosite as an efficient option to reduce the potential leaching of Mo in FA leachates; this was owing to its irregular sorption behaviour in the presence of the $CO_{2\ (g)}$ flow that was required to maintain a low pH. Moreover, injecting $CO_{2\ (g)}$ into fly ash leachates failed to reduce the pH below 4.5.

A novel chemical stabilisation method based on a Fly ash: portlandite aggregates induced the immobilisation/fixation primarily of both Mo and Ni and also of As and Se, sufficiently to reduce their concentration in the leachates to below the limits established by the European Council Decision (2003/33/EC), which supports the use of this aggregate to reduce FA pollutants. The fixation mechanism for Mo and Ni in the fly ash: portlandite aggregates could be due to the precipitation of the $CaMoO_4$ and $NiMoO_4$ phases, respectively.

The resulting FA: portlandite aggregate product could be then used as a substitute for concrete production, which would increase the ecological and technological benefits of this by-product. Future work will be focused on the evaluation of the FA: portlandite aggregate product as a substitute for sand in concrete production.

The findings of this study can therefore directly contribute to the future environmental health and social and economic development of various countries as they make important decisions on electricity generation while striving to develop industry.

## CRediT authorship contribution statement

**Patricia Córdoba**: Conceptualization, Formal analysis, Methodology, Writing – Original draft, modelling, review and editing, Supervision. **Carlos Ayora**: Data curation, Formal Analysis, Writing - review and editing. **Xavier Querol**: Writing - review and editing.

## Declaration of Competing Interest

The authors declare that they have no known competing financial interests or personal relationships that could have appeared to influence the work reported in this paper.

## Acknowledgements

We would like to thank the staff of the power station for their support, help, and kind assistance. We wish to also thank the analytical assistance of Mercè Cabañas and Silvia Martinez (Institute of Environmental Assessment and Water Research, Spanish National Research Council, IDÆA-CSIC). The corresponding author also gratefully acknowledges IDAEA-CSIC and the Excelencia Severo Ochoa Project (CEX2018-000794-S), financed by the Ministry of Science and Innovation (MINECO, Spain) and by the Generalitat de Catalunya (AGAUR 2017 SGR41).

## Appendix A. Supporting information

Supplementary data associated with this article can be found in the online version at doi:10.1016/j.ecoenv.2020.111488.

## References

Anthony, E.J., Jia, L., Burwell, S.M., 2003. PetroleumCoke FBC Ash: a Detailed Look at Calcium in the Ash. ASME FBC2003–f2172, pp. 613-620, 10.1115/FBC2003-172.

Anthony, E.J., Jia, L., Burwell, S.M., Najman, J., Bulewicz, E.M., 2006. Understanding the behavior of calcium compounds in petroleum coke fluidized bed combustion (FBC) ash. J. Energy Resour. Technol. 128, 290–299. https://doi.org/10.1115/1.2358144.

Baeyens, B., Bradbury, M.H., 1998. A mechanistic description of Ni and Zn sorption on Na-montmorillonite. Part I: titration and sorption measurements. J. Cont. Hydrol. 27, 199–222.

Barling, J., Anbar, A.D.D., 2004. Molybdenum isotope fractionation during adsorption by manganese oxides. Earth Planet. Sci. Lett. 217, 315–329. https://doi.org/10.1016/S0012-821X(03)00608-3.

Bryers, R.W., 1995. Utilization of petroleum coke and petroleum blends as a means of steam raising coke/coal. Fuel Processing Technology 44, 121–141.

Chappaz, A., Gobeil, C., Tessier, A., 2008. Geochemical and anthropogenic enrichments of Mo in sediments from perennially oxic and seasonally anoxic lakes in Eastern Canada. Geochim. Cosmochim. Acta 72, 170–184. https://doi.org/10.1016/j.gca.2007.10.014.

Chen, L., Dick, W.A., Kost, D., 2006. Circulating fluidized bed combustion product addition to acid soil: alfalfa (***Medicago sativa*** L.) composition and environmental quality. J. Agric. Food Chem. 54, 4758–4765. https://doi.org/10.1021/jf0603275.

Chen, L., Kost, D., Dick, W.A., 2010. Petroleum coke circulating fluidized bed combustion product effects on soil and water quality. Soil Sci. 175, 270–277. https://doi.org/10.1097/SS.0b013e3181e284c0.

Córdoba, P., Font, O., Izquierdo, M., Querol, X., Leiva, C., López-Antón, M.A., Díaz-Somoano, M., Martínez-Tarazona, M.R., Ochoa-González, R., Gómez, P., 2012. The retention capacity for trace elements by the flue gas desulphurisation system under operational conditions of a co-combustion power plant. Fuel 102, 773–778.

Council Decision 2003/33/EC of 19 December 2002 establishing criteria and procedures for the acceptance of waste at landfills pursuant to Article 16 of and Annex II to Directive 1999/31/EC.

Cui, J., Duan, L., Zhou, L., Zhao, C., 2018. Effects of air pollution control devices on the chlorine emission from 410 t/h circulating fluidized bed boilers co-firing petroleum coke and coal. Energy Fuels 2018, 32–4416. https://doi.org/10.1021/acs.energyfuels.7b03106.

Díaz-Somoano, M., Unterberger, S., Hein, K.R.G., 2006. Prediction of trace element volatility during co-combustion processes. Fuel 85, 1087–1093.

Felmy, A.R., Rai, D., Mason, M.J., 1992. The solubility of $CaMoO_4$ (c) and an aqueous thermodynamic model for Ca2+-MoO24-ion-interactions. J. Solut. Chem. 21, 525–532. https://doi.org/10.1007/BF00649561.

Flisowska, J., Moore, C., 2019. Climate Action Network (CAN) Europe and Sandbag. (Accessed June 2020) ⟨http://www.caneurope.org/docman/coal-phase-out/3545-just-transition-or-just-talk/file⟩.

Font O., Izquierdo M., Álvarez-Ayuso E., Moreno N., Diez S., Querol X., Otero P., Ballesteros J. C., Gimenez A., Huggins F.E. , 2007. Effect of the addition of petcoke on the partitioning of trace elements in pulverised coal combustion (PCC) plants. Proceedings: World of Coal Ash Conference. Kentucky, U.S.A.

Goldberg, T., Archer, C., Vance, D., Poulton, S.W., 2009. Mo isotope fractionation during adsorption to Fe (oxyhydr)oxides. Geochim. Cosmochim. Acta 73, 6502–6516.

Goldberg, S., Forster, H.S., Godfrey, C.L., 1996. Molybdenum adsorption on oxides, clay minerals, and soils. Soil Sci. Soc. Am. J. 60, 425–432. https://doi.org/10.2136/sssaj1996.03615995006000020013x.

Guo, B., Nakama, S., Tiana, Q., Pahlevia, N.D., Hub, Z., Sasakia, K., 2019. Suppression processes of anionic pollutants released from fly ash by various Ca additives. J. Hazard. Mater. 371, 474–483.

Gustafsson, J.P., 2003. Modelling molybdate and tungstate adsorption to ferrihydrite. Chem. Geol. 200, 105–115. https://doi.org/10.1016/S0009-2541(03)00161-X.

Hartuti, S., Hanum, F.F., Takeyama, A., Kambara, S., 2017. Effect of additives on arsenic, boron and selenium leaching from coal fly ash. Minerals 7 (6), 99. https://doi.org/10.3390/min7060099.

Izquierdo, M., Font, O., Moreno, N., Querol, X., Huggins, F., Álvarez-Ayuso, E., Diez, S., Otero, P., Ballesteros, J.C., Gimenez, A., 2007. Influence of a modification of the petcoke/coal ratio on the leachability of fly ash and slag produced from a large PCC power plant. Environ. Sci. Technol. 41, 5330–5335.

Jeong, Y., Fan, M., Singh, S., Chuang, C.L., Basude, S., J. Hans, van L., 2007. Evaluation of iron oxide and aluminium oxide as potential arsenic(V) adsorbents. Chem. Eng. Process. - Process. Intensif. 46 (10), 1030–1039.

Kaback, D.S., Runnells, D.D., 1980. Geochemistry of molybdenum in some stream sediments and waters. Geochim. Cosmochim. Acta 44, 447–456. https://doi.org/10.1016/0016-7037 (80)90043-5.

Lieberman, R.N., Green, U., Segev, G., Polat, M., Mastai, Y., Cohen, H., 2015. Coal fly ash as a potential fixation reagent for radioactive wastes. Fuel 153, 437–444.

Lieberman, R.N., Knop, Y., Izquierdo, M., Moreno, N., de la Rosa, J., Cohen, H., Muñoz-Quiros, C., Córdoba, P., Querol, X., 2018. Potential of hazardous waste encapsulation in concrete with coal fly ash and bivalve shells. J. Clean. Prod. 185, 870–881.

Moreno, N., Querol, X., Andres, J.M., Stanton, K., Towler, M., Nugteren, H., Janssen-Jurkovicova, M., Jones, R., 2005. Physico-chemical characteristics of European pulverised coal combustion fly ashes. Fuel 84, 1351–1363.

Nugteren, H., 2010. Secondary Industrial Minerals from Coal Fly ash and Aluminium Anodising Waste Solutions (PhD thesis), ISBN 978-90-5335-351-6.

Olmeda, J., Rojas, M.I.S., Frias, M., Donatello, S., Cheeseman, C.R., 2013. Effect of petroleum (pet) coke addition on the density and thermal conductivity of cement pastes and mortars. Fuel 107, 138–146. https://doi.org/10.1016/j.fuel.2013.01.074.

Parkhurst, D.L., Appelo, C.A.J., 1999. User's Guide to PHREEQC (version 2). A Computer Program for Speciation, Reaction-path, 1d-transport, and Inverse Geochemical Calculations. US Geol. Surv., p. 312. Water Resour. Inv. Rep. 99-4259.

Petroleum Coke (Fuel-grade) Market Report Insights and Industry Analysis by Application (Cement, Power Plant, Brick and Glass, Paper and Pulp, Foundaries), and Region, Competitive Market Size, Share, Trends, and Forecast, 2018–2025.2020 Market Research Future. ⟨https://www.marketresearchfuture.com/reports/petroleum-coke-market-6566⟩. (Accessed June 2020).

Querol X., Alastuey A., Chinchón J.S., Fernández J.L., López A. 2nd Report7220/Ed/014 European Coal and Steel Community project, 1993.

Rask, E., 1985. Mineral Impurities in Coal Combustion. Behaviour Problems and Remedial Measures. Springer-Verlag, Berlin.

Rodak, B.W., Siqueira-Freitas, D., de Oliveira Lima, G.J.E., Rodrigues do Reis, A., Schulze, J., Guimarães, Guilherme, L.R., 2018. Beneficial use of Ni-rich petroleum coke ashes: product characterization and effects on soil properties and plant growth. J. Clean. Prod. 198, 785–796.

Spears, D.A., Martínez-Tarrazona, M.R., 2004. Trace elements in combustion residues from a UK power station. Fuel 483, 2265–2270.

Wang, L., Feng, X., Shen, L., Jiang, S., Gu, H., 2019. Carbon and sulfur conversion of petroleum coke in the chemical looping gasification process. Energy 179, 1205–1216.